Improved thermal energy storage of nanoencapsulated phase change materials by atomic layer deposition

Nuria Navarrete[1], Damiano La Zara[2], Aristeidis Goulas[2], David Valdesueiro[3], Leonor Hernández[1], J. Ruud van Ommen[2], Rosa Mondragón[1*]

[1] Departamento de Ingeniería Mecánica y Construcción, Universitat Jaume I, 12071-Castellón de la Plana, Spain

[2]Department of Chemical Engineering, Delft University of Technology, 2629 HZ, Delft, The Netherlands.

[3] Delft IMP B.V, Molengraaffsingel 10, 2629 JD, Delft, the Netherlands

**Corresponding author: mondragn@uji.es*

ABSTRACT

Renewable energy has become of great interest over the past years in order to mitigate Global Warming. One of the actions gaining attention is the enhancement of the thermal energy storage capacity of Concentrated Solar Power plants. The addition of nanoencapsulated phase change materials (core-shell nanoparticles) to the already used materials has been proposed for that purpose, due to the possibility of increasing thermal storage through the contribution of both core latent heat and sensible heat. In this work, Atomic Layer Deposition has been used to synthesise SiO_2 and Al_2O_3 nanoscale coatings on tin nanoparticles. The multi-encapsulated phase change materials have been characterised in terms of chemical composition, crystalline structure, particle size, thermal stability and thermal storage capacity. $Sn@Al_2O_3$ nanoparticles present the best thermal behaviour as they show the lowest reduction in the phase change enthalpy over 100 cycles due to the oxidation barrier of the coating. Moreover, the specific heat of both nanoparticles and solar salt-based nanofluids is increased, making the nanoencapsulated phase change material suitable for thermal energy storage applications.

Keywords: Phase Change Material, Nanoencapsulation, Thermal Energy Storage, Atomic Layer Deposition

1. Introduction

The general trend in the energy field is moving towards renewable energy. One of the key issues for its use is improving the possibilities for energy storage, in order to overcome the intermittencies of availability of the energy sources [1, 2]. In the case of Concentrated Solar Power (CSP) plants, the most featured mechanism for this purpose is the installation of a Thermal Energy Storage (TES) system based on two tanks of molten salts, one hot and one cold, that can keep the plant active when there is no sunlight available [3, 4].

Also very important in the storage of thermal energy is the use of Phase Change Materials (PCMs) [5–7]. These materials have high phase change enthalpies, that is to say, they absorb a considerable amount of energy in order to melt, and this energy remains stored within the material until it is released to the medium again when the PCM solidifies. Among the different kinds of existing PCMs, metals and metallic alloys generally present some advantages. Besides high latent heat, they normally have high thermal conductivity, which makes energy charge and discharge cycles faster [8].

Although the most studied applications for PCMs so far are as TES technologies in solar thermal and waste heat energy, their interest is increasing in other industrial areas such as thermal regulation in photovoltaic-thermoelectric systems, products that require low-temperature storage, electronic parts that are temperature-sensitive, energy saving in thermoregulated building materials or textiles, etc. [9]

Regarding their use in energy storage, one way to introduce metallic PCMs as a heat storage medium within the current TES technologies, such as molten salts storage in CSP, is the use of nanofluids with PCMs as nanoparticles dispersed in the salts. Nanofluids are colloidal suspensions of particles between 1 and 100 nm, which allow to

partially include the physical properties of a solid, while keeping the transport properties of the fluid to a certain extent. The key issue with nanofluids is that, given the small size of the particles, they can remain suspended within the fluid instead of settling, as the Brownian motion can overcome gravity forces [10, 11].

Therefore, a nanofluid containing molten salts as the base fluid and metallic PCMs as the solid nanoparticles could serve as an enhanced way of thermal storage, contributing with the addition of the latent heat storage provided by the nanoencapsulated PCM (nePCM) cores. Moreover, in this application, metallic nanoparticles also present the advantage of their high density, which allows for considerable improvements in the thermal properties (that depend on the mass loading), without excessively increasing the viscosity (that depends on the volumetric concentration). Besides the latent heat storage capacity, the addition of nanoparticles to molten salts has been proved to increase the sensible heat storage capacity of the mixture due to the interactions between the nanoparticle and the fluid [12–14]. For this reason, both the phase change enthalpy and specific heat of the nanoparticles and nanofluids need to be optimized for thermal storage applications.

However, it must be considered that in order to use a PCM as the solid phase in a nanofluid the nanoparticles must have a core-shell structure, that is to say, the PCM must be encapsulated by a high melting point material, which will prevent the different particles from collapsing into each other when the PCM is melted [15–17]. Metallic nanoparticles usually present a native thin oxide layer formed by passivation in contact with air, which can serve as self-encapsulation in some cases [18,19]. Nevertheless, further oxidation of the cores material can take place due to interactions with the base fluid or when the particles are exposed to high temperatures or thermal cycling, decreasing the energy stored through latent heat by the nePCMs. Therefore, this work

deals with the possibility of engineering a multi-layered encapsulation of the particles, synthesising a second nanoscale coating of an insulating material using atomic layer deposition.

Atomic layer deposition (ALD) is a gas-phase deposition technique [20] that has been utilized for the alteration of surface properties of both micron- and nano-sized metallic particles with minimal influence of their bulk properties. The uncoated nanoparticles are cyclically exposed to two gaseous precursors that chemisorb on their surface. A purging step is needed to remove the unreacted molecules after every exposure to the different precursors in order to avoid undesired gas-phase reactions between them. Hence, the deposition process is highly controlled, and films of a few nanometres whose thickness can be tuned by varying the number of cycles of precursor exposure can be synthesised. Processing of transition (Ni [21–26], Fe [23, 24, 27–30], Cu [23, 30] and Co [23]) and post-transition metal particles (Al [24, 31–33], Zn [24] and W [34] has been reported through ALD. Several oxide (Al_2O_3 [21–24, 26–28, 30, 34], TiO_2[23, 25, 29], SnO_2 [31, 32], Fe_2O_3 [33], and ZnO [32]), nitride (BN [24]) and composite (Al_2O_3/ZnS [27] and AlN/TiO_2 [29]) ALD coatings have been deposited; for an overview see Miikkulainen et al. Different ALD processes have different values for the growth-per-cycle (GPC). For the case of Al_2O_3 synthesised using trimethylaluminum (TMA) and water the values range between 0.1-0.2 nm [34]. Due to the oxidation avoidance prerequisites, relatively mild processing conditions in terms of temperature (up to 350 ^oC) and co-reactant reactivity (mostly H_2O or H_2O_2) are preferred. Agitated reactor vessels such as fluidized beds [21, 35] and rotary reactors [30, 34] provide favorable coating conformality and uniformity characteristics as compared to viscous flow [32] or flow-type [25] reactors.

In this work, we aim to deposit SiO_2 and Al_2O_3 coatings on commercial Sn nanoparticles with a thin SnO_x passivating layer by using fluidized bed ALD. The

presence of the nanolayer and its chemical composition were determined in order to evaluate the performance of the ALD technique to coat this kind of material. Finally, the performance of the ALD coatings, which are meant to prevent the further oxidation of the nePCM cores when exposed to working conditions, such as interaction with the base fluid or thermal cycling, has been tested through thermal characterization of the enhanced nePCMs and the Solar Salt based nanofluids containing them.

2. Materials and methods

Materials

Commercial Sn nanoparticles of nominal size <300 nm were purchased from US Research Nanomaterials, Inc. These nanoparticles were produced by the electro-physical fumed combined with strong airflow injection method. The phase change enthalpy and temperature for bulk Sn are 59.2 kJ/kg and 232 ºC respectively.

Regarding the ALD process, the Al precursor, trimethylaluminum (TMA), was purchased from Akzo Nobel HPMO in a 600 mL stainless steel bubbler canister. The Si precursor, silicon tetrachloride ($SiCl_4$), was purchased from Sigma-Aldrich. Demineralized water was used as a co-reactant for both SiO_2 and Al_2O_3 ALD. All the precursors were contained in stainless steel bubblers and used as received.

For the synthesis of the solar salt-based nanofluids, a mixture of sodium and potassium nitrates, in a 60/40 wt.% proportion was used. The nitrates were purchased from Labkem (Analytical grade ACS), weighted in the desired proportions and mechanically blended with the nanoparticles in a 1wt.% concentration. Any trace of humidity from the salts was previously removed by placing the nitrates in an oven at 100 ºC for 20 min.

ALD Experiments

The coating experiments were carried out in an atmospheric-pressure fluidized bed reactor, consisting of a glass column with an internal diameter of 2.6 cm and a height of 50 cm. The reactor was placed on a double-motor vibration table (Paja PTL 40/40-24) operated at a frequency of 40 Hz to assist the fluidization of the nanoparticles. Two stainless steel distributor plates with pore size of 37 μm, placed at the bottom and the top of the column, were used to ensure a homogeneous gas distribution and to prevent any particle leakage from the reactor, respectively. The ALD precursors, i.e., TMA, $SiCl_4$ and H_2O, were kept at room temperature. The precursors were delivered to the reactor through two separate lines using nitrogen (N_2, 99.999 vol %) as a carrier gas; a third line for the purging gas was also connected to the reactor. The lines were kept at 30 °C above the bubbler temperatures to prevent any precursor condensation by using heating tapes placed around them. The reactor was heated by an infrared lamp with a feedback control to maintain the desired reaction temperature of 40 °C. The temperature of the powder bed was monitored by a type-K thermocouple inserted in the reactor. The off-gas of the fluidized bed was led through a series of washing bubblers containing mineral oil (Kaydol) to trap unreacted precursors and reaction by-products, and NaOH solution to neutralize chloride compounds arising from $SiCl_4$. The precursor bubblers, the lines, the reactor and the washing bottles were contained inside a closed cabinet. In case of Al_2O_3 ALD, the cabinet was blanketed with nitrogen and operated at an O_2 concentration below 6 % as a safety measure. An ALD cycle consisted of sequential exposures of $SiCl_4$-N_2-H_2O-N_2 for SiO_2 ALD, and TMA-N_2-H_2O-N_2 for Al_2O_3 ALD. Table 1 shows the exposure times for each precursor step. In each experiment, 20 g of Sn nanopowder were loaded in the reactor and fluidized with a flowrate of 1 NL/min. Each deposition process was run for 50 cycles. At the end of the 5^{th}, 10^{th} and 25^{th} cycles,

the experiment was stopped, and around 1 g of powder was sampled and stored for characterization.

Table 1. Experimental parameters of the ALD process.

ALD Process	Reaction Temperature (°C)	Precursor Exposure Time (min)	Number of cycles
SiO_2 ALD	40	0.5 ($SiCl_4$) -5 (N_2) -1 (H_2O) -5 (N_2)	5, 10, 25, 50
Al_2O_3 ALD	40	1 (TMA) -5 (N_2) -1 (H_2O) -5 (N_2)	5, 10, 25, 50

3. Characterization techniques

Scanning Electron Microscopy, SEM

A general view of the different samples was obtained with a Scanning Electron Microscope (SEM, JEOL-JSM 6510). The morphology and size of the nePCMs was observed and their composition was analysed using the integrated EDX module (Oxford INCA).

Field Emission Transmission Electron Microscopy, TEM

A Field Emission Transmission Electron Microscope JEM 2100F (JEOL) operating at an accelerating voltage of 200 kV was used for the visualization of the size, morphology and film thickness of the different nePCMs.

The microscope comprises a high resolution CCD camera (SC200, GATAN), and is equipped with a STEM unit with the bright field imaging detector and the high-angle annular dark-field (HAADF) detector, which enables the observation of contrast in phases with different atomic numbers. Chemical characterisation can also be performed

by the EDS X-Max 80 detector (Oxford Instruments) to determine the elemental composition of the coated nanoparticles.

Inductively coupled plasma mass spectrometry, ICP-OES

The mass loading of Al and Si in the coated samples was measured by inductively coupled plasma optical emission spectrometry (ICP-OES). Approximately 30 mg of the sample were destructed in 4.5 ml 30% HCl + 1.5 ml 65% HNO_3 + 1 ml 40% HF using a microwave oven. The destruction time in the microwave oven was 60 min at maximum power. After destruction, the samples were diluted to 50 ml with MQ H_2O. The destructed samples were analysed with a PerkinElmer Optima 5300DV and PerkinElmer Optima 4300DV (PerkinElmer, Waltham, MA, USA) optical emission spectrometers to determine the content of Al and Si, respectively.

Fourier-transform infrared spectroscopy, FT-IR

The chemical composition of the different samples was analysed using a FT/IR-6200 spectrometer (Jasco) with a spectral window of 4000–400 cm^{-1} in transmission mode. A small amount of sample (~1 wt.%) was mixed with KBr (IR spectroscopy grade, Scharlab SL), grounded and pressed into pellets of 13 mm of diameter.

X-ray powder diffraction, XRD

The composition and crystalline structure of the nePCMs with different coatings was analysed using a Bruker D8 X-ray diffractometer with Cu Kα radiation by studying the angles from $2\theta = 5°$ to $2\theta = 80°$ with a 0.02° step. Spectra were registered at 30 ºC, after 30 min at 280 ºC and again after cooling down to 30 ºC in order to determine the possible changes in the crystalline structure of the nePCMs when subjected to high temperature and thermal cycling.

Dynamic Light Scattering, DLS

The particle size distribution of the different nePCMs suspended in water was studied with a VascoFLEX particle size analyser (Cordouan Technologies). The device consists of an external laser head that contains the light emitter and receiver (65 mW-658 nm fiber pigtailed laser). The light registered corresponds to backscattering with an angle of 170°. In order to measure the particle size distribution closer to the primary size, avoiding the formation of agglomerates, a very dilute suspension was prepared with 32 mg of each nePCM added to 40 mL of distilled water. The nanofluids were sonicated during 5 min (Sonopuls HD2200, Bandelin electronic GmbH & Co.) and DLS measurements were carried out in a quartz cuvette of 2 mL. Three measurements were taken of each sample to ensure repeatability.

Thermogravimetric analysis, TGA

Changes on the oxidation state have been studied for all the nePCMs with thermogravimetric analysis. A TGA 1 (Mettler Toledo) was used with air atmosphere. The temperature of each sample was kept at 70 ºC for 5 minutes, then raised to 280 ºC at a 5 ºC/min rate, and held at 280 ºC for 30 min, while measuring all the changes in mass taking place. Approximately 20 mg of sample were introduced in an aluminium crucible for each test.

Differential scanning calorimetry, DSC

Information about the melting temperatures and phase change enthalpies of the nePCMs was obtained by differential scanning calorimetry (DSC2, Mettler Toledo). Samples of around 20 mg were analysed in 40 µl aluminium crucibles. They were studied from 70 ºC to 280 ºC and back to 70 ºC with heating and cooling rates of 5 ºC/min and 5 min isothermal steps at the minimum and maximum temperatures. The samples were also

subjected to thermal cycling, repeating this program 100 times. All these tests were performed under inert atmosphere, with a constant 25 mL/min N_2 flow rate.

The nePCMs were also subjected to 5 thermal cycles under air atmosphere to evaluate the influence of oxygen exposure on the thermal properties.

Heat impact resistance of the nePCMs was studied by submitting the samples to fast thermal cycles. Two initial cycles from 70 ºC to 280 ºC and back to 70 ºC with heating and cooling rates of 5 ºC/min and 5 min isothermal steps at the minimum and maximum temperatures were applied to check the initial behaviour. Then they were subject a similar cycle with heating and cooling rates of 100 ºC/min. The samples were then exposed to air atmosphere, so if there was any leakage of the cores pure Sn it would oxidise, and later, two more slow thermal cycles were applied to observe the possible alterations in the nePCMs melting behaviour. This procedure was then repeated reaching a maximum temperature of 450 ºC in the fast cycle.

The specific heat of the nePCMs and nanofluids based on their mixture with Solar Salt was also measured with DSC. The *areas method* [36] was used to study specific heat at 80 ºC and 180 ºC, when Solar Salt and nePCMs are still in solid state, at 280 ºC, when both Solar Salt and the nePCMs cores are in molten state, and back at 180 ºC, when the nePCMs cores are still melted due to supercooling but the solar salt has already solidified. A standard sapphire was tested prior to each sample, using the same cycle procedure, with a 1 ºC step at each of the temperatures studied and 5 min isotherms before and after the step. All the specific heat tests were carried out with a constant 25 mL/min N_2 flow rate. In order to ensure repeatability at least three samples were prepared of each nePCM/nanofluid. For each one, two cycles were run in order to obtain a mean value. The experimental error was statistically obtained at a 95% of confidence

level, with a mean error of 6.87% for the nePCMs and of 2.58% for the solar salt based nanofluids.

Table 2. Summary of the tests performed over each sample.

	Sample								
Experiment	Sn	$Sn@SiO_2$				$Sn@Al_2O_3$			
# cycles	0	5	10	25	50	5	10	25	50
SEM + EDX	●				●				●
TEM + EDX (linear)	●				●		●		●
ICP-OES	●	●	●	●	●	●	●	●	●
FT-IR	●				●				●
XRD	●				●				●
DLS	●		●		●		●		●
TGA	●		●		●		●		●
Thermal cycling (5 cycles in air)	●		●		●		●		●
Thermal cycling (100 cycles, N_2)	●				●				●
Heat impact resistance	●				●				●
Specific heat	●				●				●
Specific heat with solar salt	●				●				●

4. Results and discussion

4.1 Morphology, encapsulation and chemical composition

The different nePCMs were visualised using SEM. In Figure 1, a general overview of the samples is depicted. It is observed that the particles are spherical in all the cases and the encapsulation process after 50 ALD cycles has no effect on the morphology of the particles.

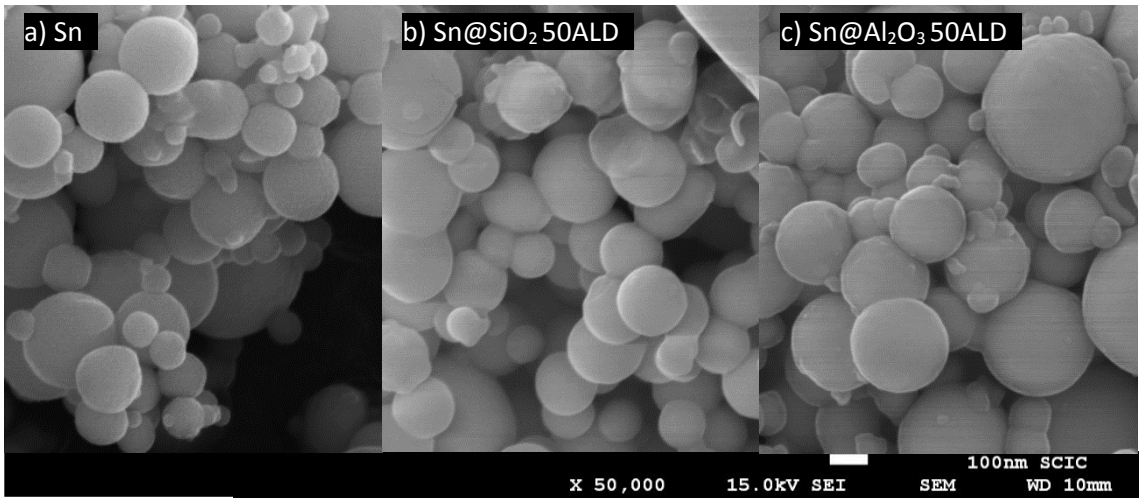

Figure 1. SEM micrographs of the nePCMs of a)Sn, b)Sn@SiO_2 after 50 ALD cycles and c) Sn@Al_2O_3 after 50 ALD cycles.

Besides, Figure 2 shows the EDX analyses of all the nePCMs including the original Sn nanoparticles that already presented a passivation layer of SnO_x before the ALD coating. The peaks shown in light grey are corresponding to elements belonging to the SEM sample holder such as C, and N, and the Pt coating needed to run the analysis. Thus the elements composing the samples are determined to be Sn and O, in Figure 2 a) corresponding to Sn nePCMs; Sn, Si and O, in Figure 2 b), corresponding to the SiO_2 coated Sn nePCMs; and Sn, Al and O, in Figure 2 c), corresponding to the Al_2O_3 coated Sn nePCMs. In Figure 2 b), peaks corresponding to Cl also appear, attributed to a small quantity of residue from unreacted ALD precursors ($SiCl_4$).

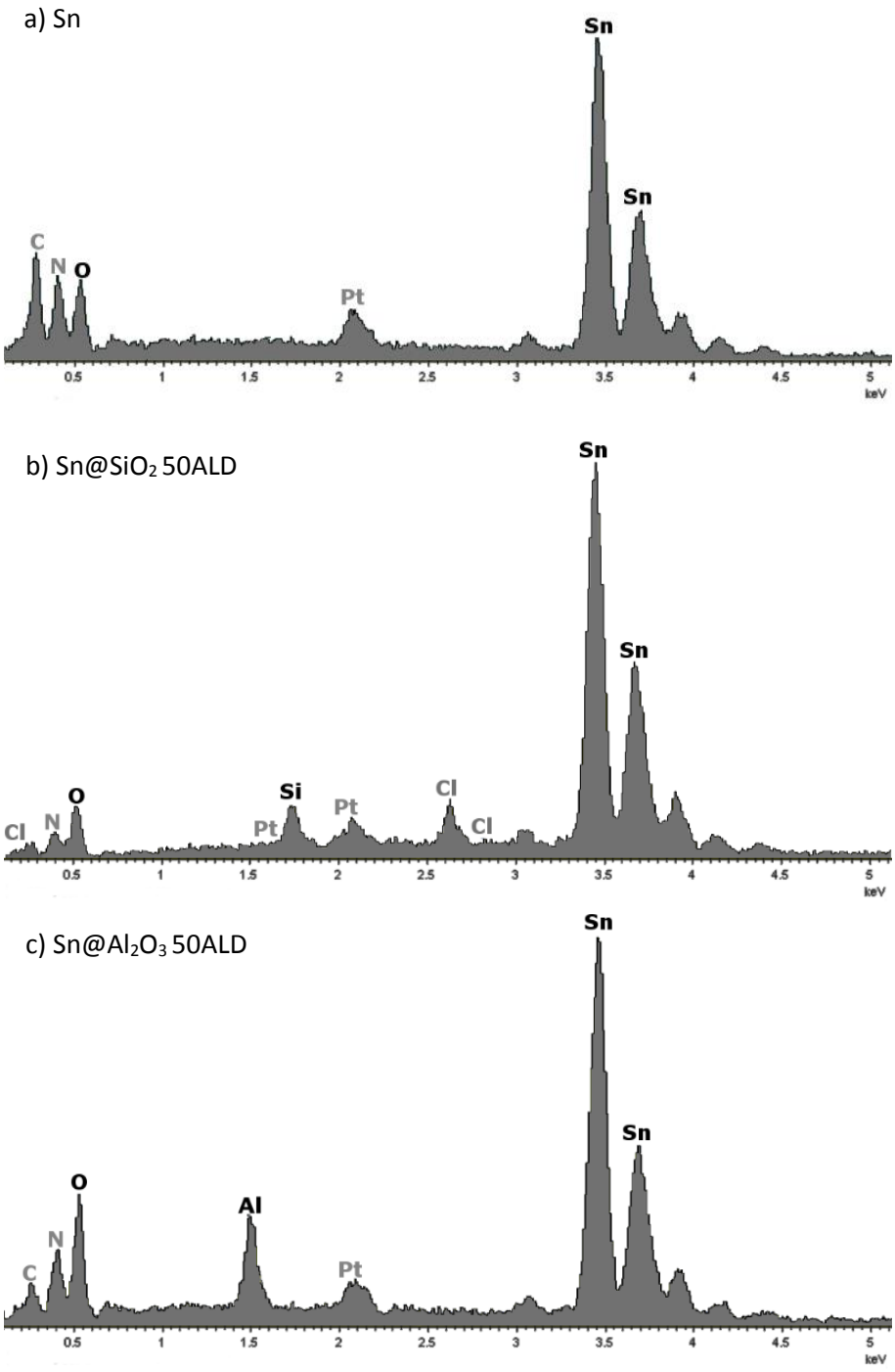

Figure 2. EDX analysis of the nePCMs of a)Sn, b)Sn@SiO_2 after 50 ALD cycles and c) Sn@Al_2O_3 after 50 ALD cycles.

The morphology of the SiO_2 and Al_2O_3 coatings on the Sn particles after 50 ALD cycles was studied using TEM. The multi-encapsulated particles can be observed in Figure 3, where the newly deposited material can be seen apart from the already present Sn cores and SnO_x passivation layer. A linear EDX analysis was performed for every nePCM, showing the composition of different the layers. Figure 3 a) shows a particle of 200 nm with a Sn core, a SnO_x passivation film of 12 nm, and a second SiO_2 ALD film of 8 nm. In Figure 3 b), the same dimensions can be observed for the particles coated with Al_2O_3, with a thickness of 10 nm of Al_2O_3 in this case. Such SiO_2 and Al_2O_3 film thicknesses translate into GPCs of 0.16 nm and 0.2 nm, respectively, which are in agreement with the values reported in literature [34, 37]. Both oxide ceramic coatings of SiO_2 and Al_2O_3 are very conformal, and fully confine the nePCM with a constant layer thickness.

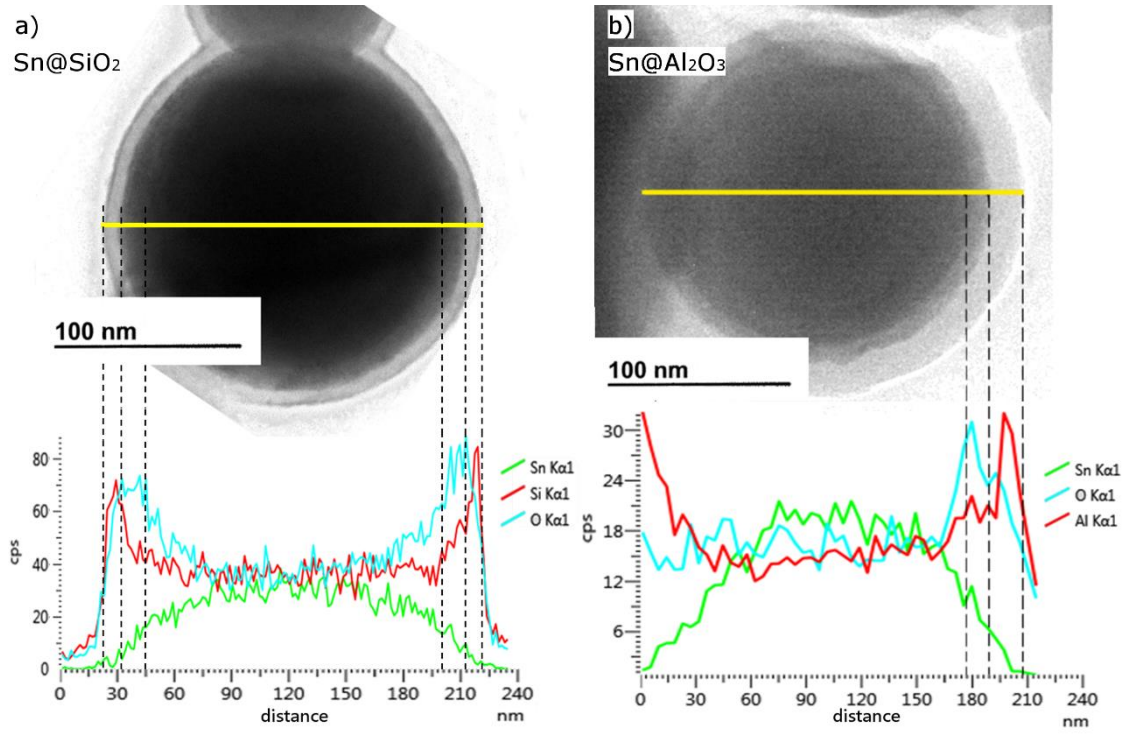

Figure 3. TEM images and EDX analysis of SiO_2 and Al_2O_3 coated Sn nePCM.

In addition to the EDX analysis, the presence of SiO_2 and Al_2O_3 on the coated nePCMs was also confirmed by FT-IR. As can be seen in Figure 4, after the coating process new

peaks appear in the infrared spectra corresponding to the SiO_2 and Al_2O_3 bonds [38]. In particular, the signatures of SiO_2 are featured by the two peaks in the wavenumber range of 1125-1200 cm^{-1}, while Al_2O_3 gives the characteristic Al-O stretching at 912 cm^{-1} [39].

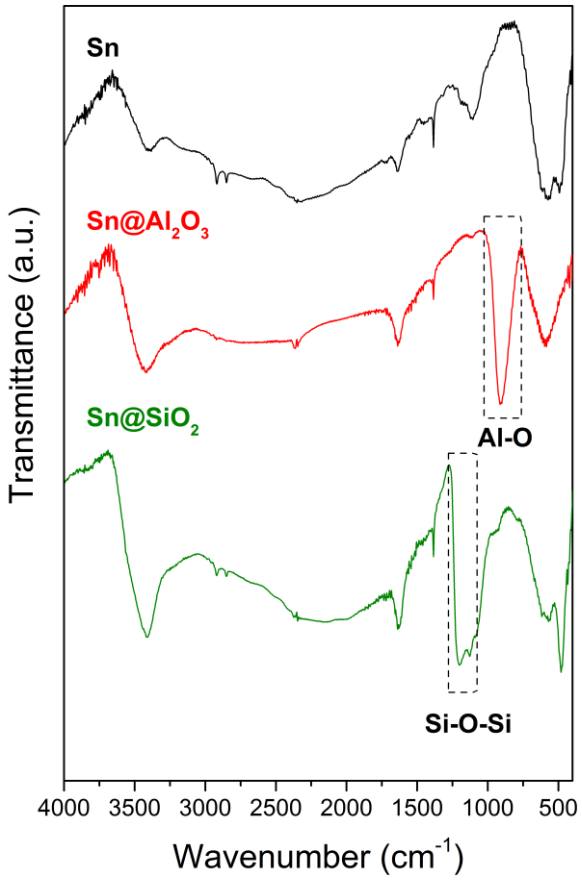

Figure 4. FT-IR spectra of the nePCMs.

The composition of the ALD coated samples was studied with ICP-OES. The mass percentages of Al and Si were measured and converted to Al_2O_3 and SiO_2 mass percentages using stoichiometry relations. The results of this analysis are plotted in Figure 5. The weight content of both SiO_2 and Al_2O_3 in the multi-coated nePCMs linearly increases with the number of cycles. In particular, the maximum fraction of Al_2O_3 and SiO_2 in the samples after 50 ALD cycles was 3 %wt. and 1.3 ± 0.3 %wt., respectively.

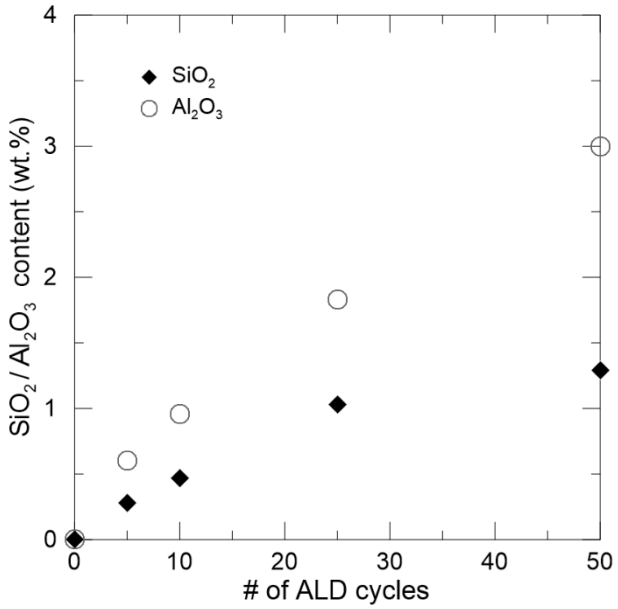

Figure 5. Evolution of SiO_2/Al_2O_3 deposited with number of cycles

The different crystallographic phases present in the $Sn@SiO_2$ and $Sn@Al_2O_3$ samples were studied by X-Ray Diffraction. The samples were analysed initially at 30 ºC, then the temperature was raised to 280 ºC, and then they were analysed again at 30 ºC. The results of the diffraction are shown in Figure 6.

For the $Sn@SiO_2$ nePCMs, it can be observed that initially only the peaks belonging to pure Sn cores appear, therefore it is crystalline, while the SnO_x and SiO_2 of the multi-layered encapsulation are amorphous. After the heating of the sample at 280 ºC, the core material is melted, and thus it does not appear in the diffractogram. However, it can be noticed that the SnO_x layer has crystallised and its structure is that of SnO_2, unlike that of the initial Sn/SnO particles [18]. This change on the oxidation state is assumed to take place due to the SiO_2 coating, since it does not occur for the Al_2O_3 coated nePCMs. Finally, after the sample was cooled back down to 30 ºC, both Sn and SnO_2 peaks appear, while SiO_2 is still amorphous.

The results obtained for the $Sn@Al_2O_3$ nePCMs are similar. Initially, only the Sn cores are crystalline at 30 ºC. After heating the sample at 280 ºC the tin oxide layer crystallised to SnO, and both Sn and SnO spectra are present after the cooling down of

the sample to 30 ºC. Therefore, it can be determined that both the SiO_2 and the Al_2O_3 coatings deposited on the Sn nePCMs are amorphous.

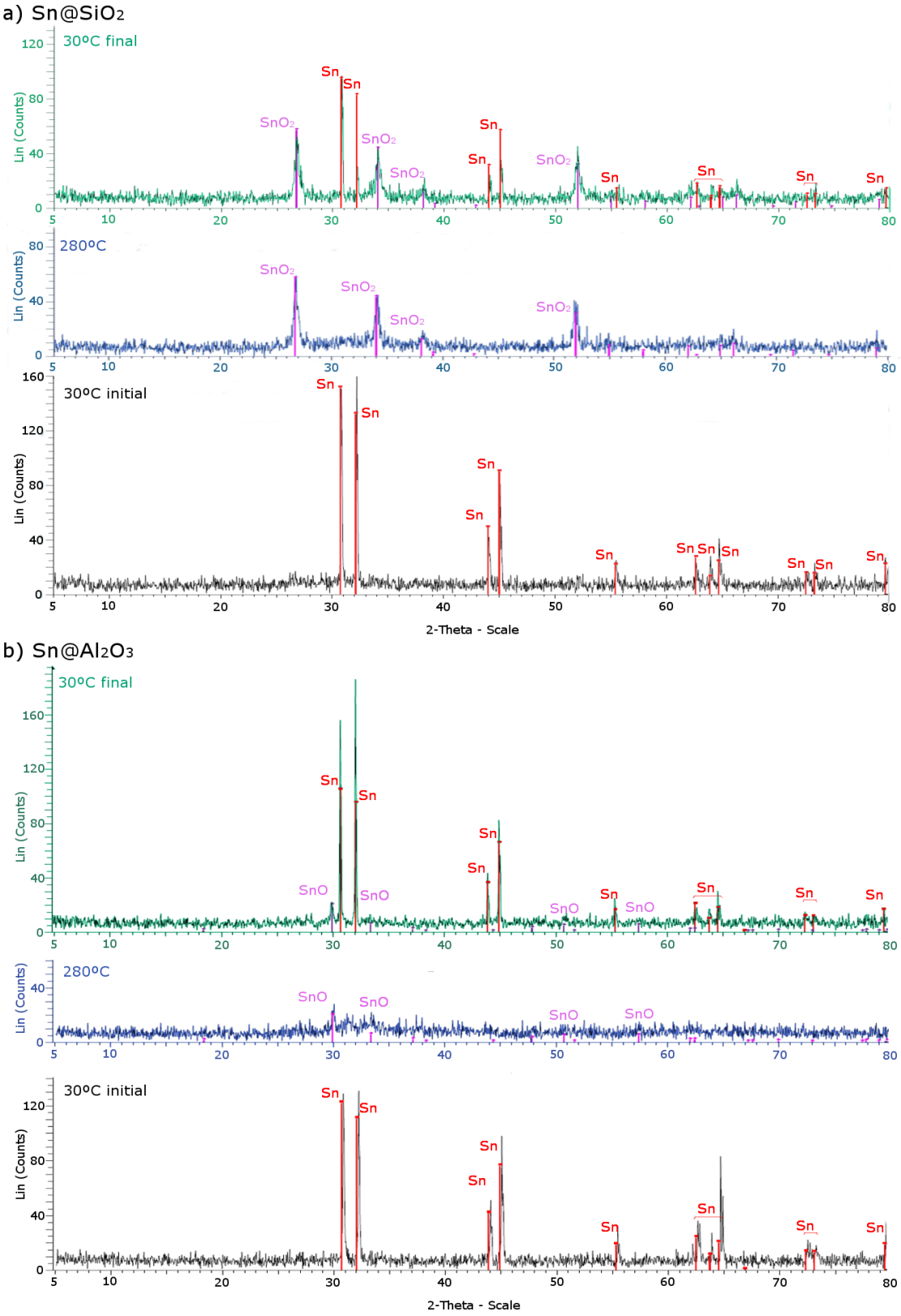

Figure 6. XRD diffractograms of the a)SiO_2 and b)Al_2O_3 coated nePCMs.

4.2 Particle size

The possible alterations of the nePCMs size or sintering of the nePCMs during the ALD process was studied by dispersing a very small amount of the different samples in water and analysing the suspensions with DLS. The particle size distribution of the nePCMs coated with 10 and 50 ALD cycles was measured to assess the effect of the processing time on the particles. Figure 7 shows the results of the DLS analysis. The particle size distribution of all of the samples studied, regardless of the coating or the number of cycles, show two different intensity peaks. The first one corresponds to particles of around 180 nm, the mean diameter of the Sn nePCMs [18]. The second one ranges from 600 to 800 nm, and it corresponds to clusters of particles. However, this peak is also present for the Sn nePCMs before the coating process, therefore it corresponds to the agglomeration of the particles because of attractive forces. Moreover, the difference between the mean peak sizes of the samples coated for 10 and 50 cycles is minimal, proving the ALD coating process did not impact the size or the agglomeration state of the nanoparticles.

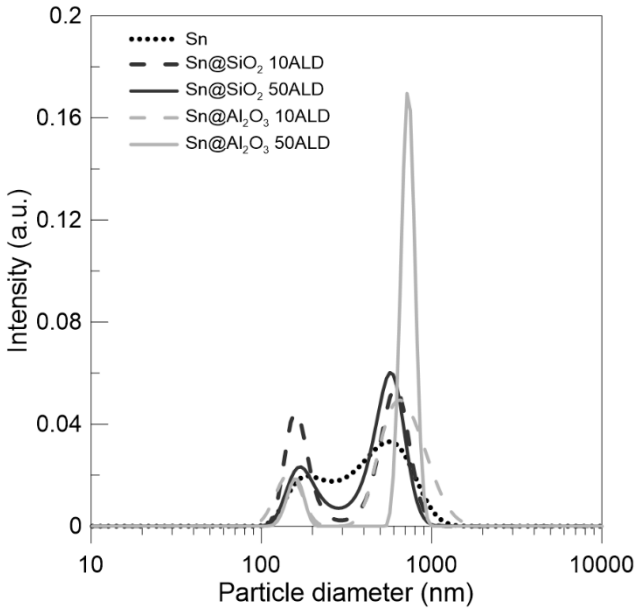

Figure 7. Particle size distribution of the nePCMs in water.

4.3 Thermal stability

In order to test the thermal stability of the multi-coated nePCMs, a TGA analysis on air was performed on the samples. Their behaviour when exposed to a progressive increase of temperature from 70 ºC and a posterior isotherm at 280 ºC is shown in Figure 8.

It is observed that the Sn nePCMs sample loses some mass at the beginning, likely corresponding to impurities present on the commercial nanoparticles (e.g. additives like anti-agglomerants commonly used in industrially produced powders). Above 200 ºC the mass starts to increase in a rather constant way. This is a sign that the nePCMs cores are oxidizing further than the initial passivation layer of SnO. This mass uptake would be a drawback for the application of these materials as a latent heat storage medium when in contact with air.

For the ALD coated nePCMs, an initial weight loss is also present. Apart from the previously mentioned impurities of the commercial nanoparticles, some residual products can be present after the ALD coating, e.g. chlorine compounds from $SiCl_4$ after the SiO_2 coating (presence of Cl has been detected in the EDX analysis performed and shown in Figure 2), and carbonaceous species from TMA after the Al_2O_3 ALD. Precursor ligand leftovers that result in a small weight loss when subject to TGA have been previously reported in the literature [40, 41]. However, the weight percentage of these impurities is very low (i.e., 0.3% mass loss difference between Sn and Sn@SiO_2 nePCMs), especially when compared to the deposition rates of the coating films previously shown in Figure 5. By optimising the deposition conditions, especially with regard to the second ALD half-reaction step, the influence of residual compounds of the precursor molecule on the coating quality could be further reduced.

After the initial weight loss, a more prominent mass gain than that of Sn nePCMs can be observed in the isothermal segment at 280 ºC for the SiO_2 coated nePCMs. Although

this could be initially attributed to the oxidation of the cores as in the previous case, it has also been observed in the XRD analysis in Figure 6 that the tin oxide present in the $Sn@SiO_2$ nePCMs is SnO_2 instead of SnO. Therefore, this mass gain taking place can be related to the change on the oxidation state.

As for the $Sn@Al_2O_3$ samples, the behaviour of the samples during the isothermal segment at 280 ºC is very stable, which indicates that the cores are not oxidizing and therefore the latent heat due to the melting of the cores remains constant.

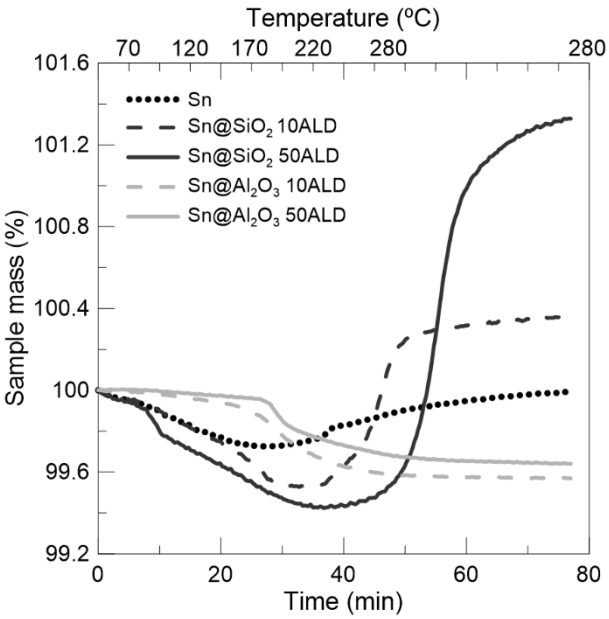

Figure 8. TGA analysis of the different nePCMs.

Heat impact resistance of the nePCMs was also tested. The samples were subject to two fast thermal cycles (with heating/cooling rates of 100 ºC/min), first up to 280 ºC, and later up to 450 ºC to check if the encapsulation could resist. In Figure 9, a comparison between the initial fusion peaks and the peaks after these heat impact cycles is depicted for each nePCM. The variation present in the fusion peaks of Sn is very small, although a certain displacement appears. However, if the nePCM could not withstand the thermal cycle applied, that would result in the breakage of the encapsulations and leaking of the core material, which would oxidise in contact with air causing a notable decrease in the

fusion enthalpy that is not observed for any of the samples. The differences observed between the initial and after the heat impact for the $Sn@SiO_2$ and $Sn@Al_2O_3$ samples are even smaller, which indicate that the nePCMs can resist fast temperature changes without losing their properties.

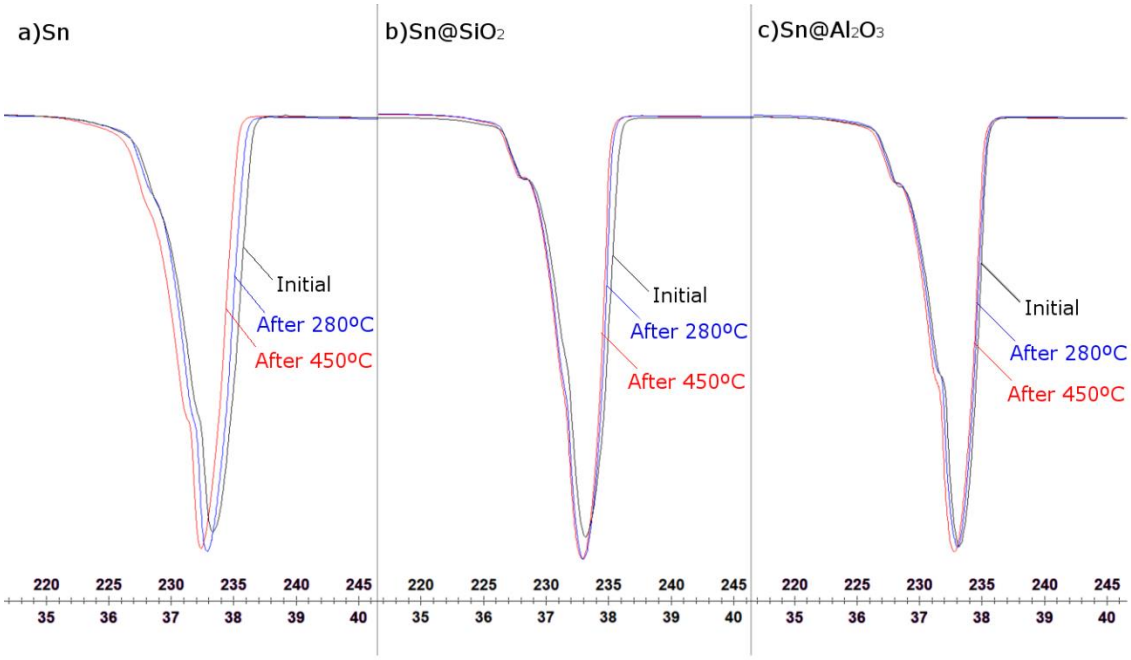

Figure 9. Heat impact resistance analysis. Comparison of the samples fusion peaks after thermal cycles of 100 ºC/min up to 280ºC and 450ºC.

4.4 Thermal energy storage capacity

The latent heat of the nePCMs was analysed by means of DSC. A complete cycle of fusion and solidification within N_2 atmosphere of each of the samples after 50 ALD cycles can be observed in Figure 10 a). It is noticed that the fusion temperature corresponding to the downward peak is constant for all samples studied, and thus not affected by the ALD process. This is also reflected in the values of the phase change enthalpies (Table 3), which are smaller for the multi-coated nePCMs. This behaviour was expected since this property depends on the ratio of pure Sn per gram of nePCM,

which decreases after the samples are coated with SiO_2 or Al_2O_3. However, this decrease is not that significant, especially in the case of the Sn@Al_2O_3 sample.

In Figure 10 b) a complete cycle of fusion and crystallization after 100 thermal cycles is depicted for each of the samples. It is observed that the fusion temperature remains the same after the cycling and there are no significant changes in the overall curves thus confirming the stability of the samples to thermal cycling.

Regarding the crystallisation temperatures, clear differences can be noticed among the samples. The difference between the fusion and crystallisation temperatures is known as supercooling and depends to a great extent on the material and size of the PCM [18, 42]. This difference occurs due to the lack of nucleation points for crystal growth during solidification, and, in this case, both Sn and Sn@Al_2O_3 have a similar crystallisation point, while Sn@SiO_2 shows a smaller value. One possibility for nucleation points are the imperfections in the interface between the nePCM core and the SnO_x layer. The difference in the temperatures could be the result of the different oxidation state of the passivation layers of the Al_2O_3 and SiO_2 coated nePCM (SnO and SnO_2 respectively), which could contain a lower number of defect in the structure for the SnO_2 interlayer, favouring the heterogeneous nucleation of the Sn crystals.

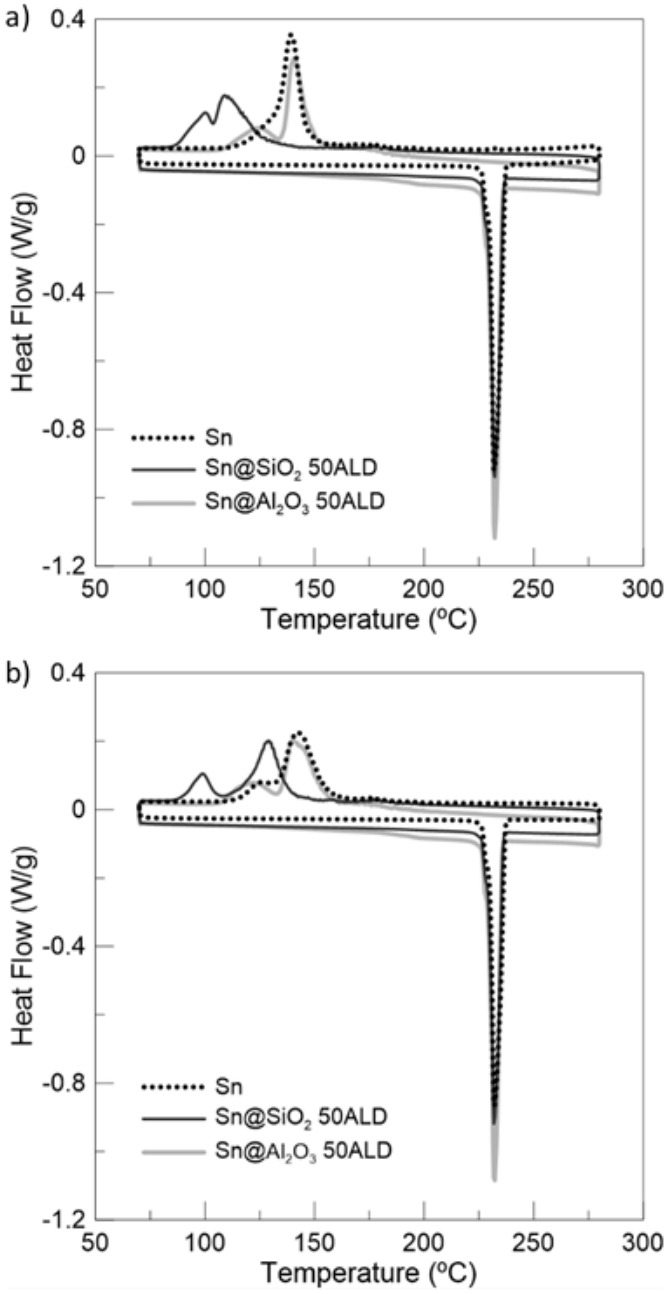

Figure 10. DSC fusion-crystallisation comparison of a) 1st cycle and b) 100th cycle.

Table 3. Phase change data from the 1st cycle of DSC analysis of the nePCMs.

Sample	Phase change enthalpy (J/g)	Fusion Temperature (ºC)	Crystallisation Temperature (ºC)
Sn	52.99	232.00	139.48
Sn@SiO_2 50ALD	48.71	232.75	123.38
Sn@Al_2O_3 50ALD	51.74	232.99	143.22

The stability of the nePCMs to thermal cycling and the suitability of the different ALD coatings as an oxidation barrier were tested by subjecting the samples first to 5 thermal cycles up to 280 ºC within an air atmosphere containing oxygen, and later, by exposing them to 100 cycles in an inert N_2 atmosphere. The evolution of the phase change enthalpy with the number of thermal cycles is plotted in Figures 11 and 12, respectively. In Figure 11, corresponding to the thermal cycling in air, it is noticeable that the SiO_2 coatings, instead of preventing the oxidation of the cores and loss of phase change enthalpy, seem to slightly promote it when compared to the uncoated Sn nePCM. However, $Sn@Al_2O_3$ samples show an enhancement in the resistance to oxidation, especially the one subjected to 50 ALD cycles, in which the phase change enthalpy remains almost constant during the 5 cycles, meaning that no oxidation of the pure Sn core is taking place even under oxidising conditions.

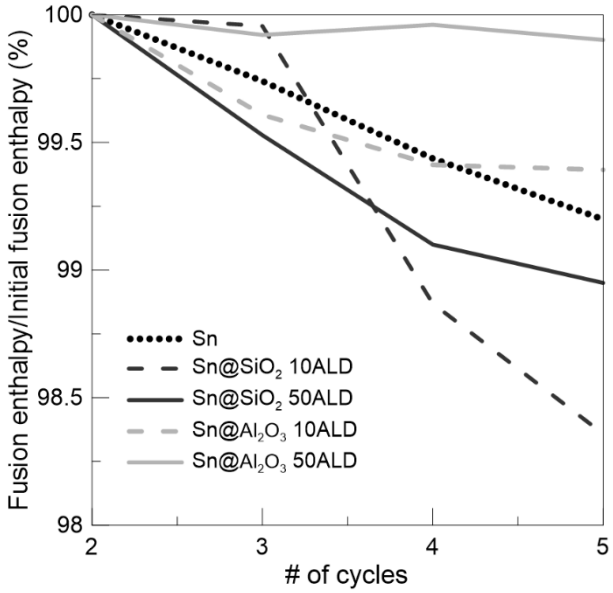

Figure 11. Evolution of the phase change enthalpy with thermal cycling in air atmosphere.

In Figure 12, corresponding to the 100 thermal cycles conducted under nitrogen, both ALD coated nePCMs show higher thermal stability than the uncoated Sn nePCMs. The

decrease of the phase change enthalpy of the Sn nePCM, up to 7%, is considerably reduced in both $Sn@SiO_2$ and $Sn@Al_2O_3$ samples.

The $Sn@Al_2O_3$ sample shows the best resistance to oxidation against thermal cycling, losing only a 1.1% of the initial phase change enthalpy, already higher than the previously obtained for the $Sn@SiO_2$ (4.1%).

Therefore, the nePCMs coated with Al_2O_3 present an overall enhancement in the oxidation resistance when exposed to thermal cycling, which implies a better performance of the nePCMs as a mean of latent heat storage in nanofluids.

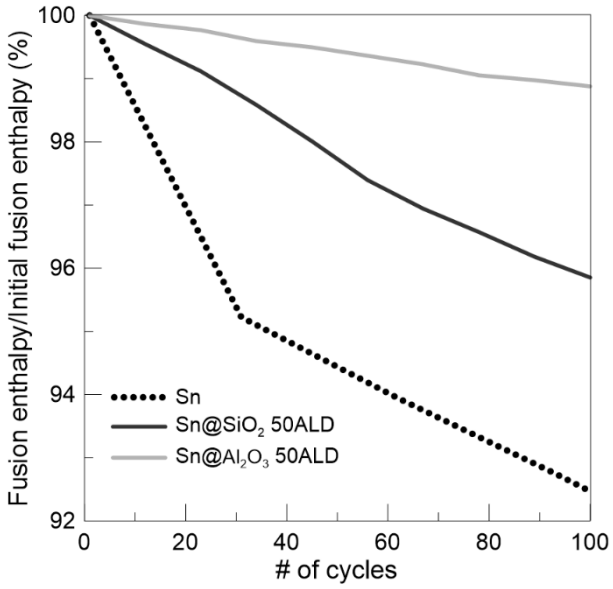

Figure 12. Evolution of phase change enthalpy with thermal cycling in nitrogen atmosphere.

Finally, the effect of the nePCMs on the specific heat of a solar salt-based nanofluid has been studied, since it is directly related to the sensible heat storage capacity of the material that is complementary to the latent heat. Figure 13 shows the values of the specific heat (C_p) of the different nePCMs and their nanofluids, prepared with a 1 wt.% concentration of particles and solar salt (SS) as the base fluid, along with their standard deviation. The variations in specific heat of the multi-coated nePCMs with respect to Sn

nePCMs, and of solar salt based nanofluids with respect to the base fluid alone are also shown in Table 4.

The variations of the specific heat of the ALD coated nanoparticles are in a range from -6.5 to +12.9%, with opposite effects of the coating material. Whereas the SiO_2 coating seems to have a detrimental effect for the $Sn@SiO_2$ at every temperature studied, the effect of the Al_2O_3 coating in the $Sn@Al_2O_3$ samples is positive, where the specific heat increases by around 10% when increasing temperature.

In the case of the nanofluids, all of the combinations show enhanced specific heats with respect to that of the solar salt, for the temperatures above 100 ºC. This enhancement is greater than what could be expected from the mixture rule, as it has been previously observed in the literature for nanofluids based on molten salts [12–14]. The enhancement is also higher for the multi-coated nePCMs with respect to the nanofluid containing the uncoated Sn nePCMs through all the temperature range studied, which means that not only the sensible heat storage will not be damaged by the addition of the multi-coated nePCMs, but it can present an enhancement of up to 11.4%.

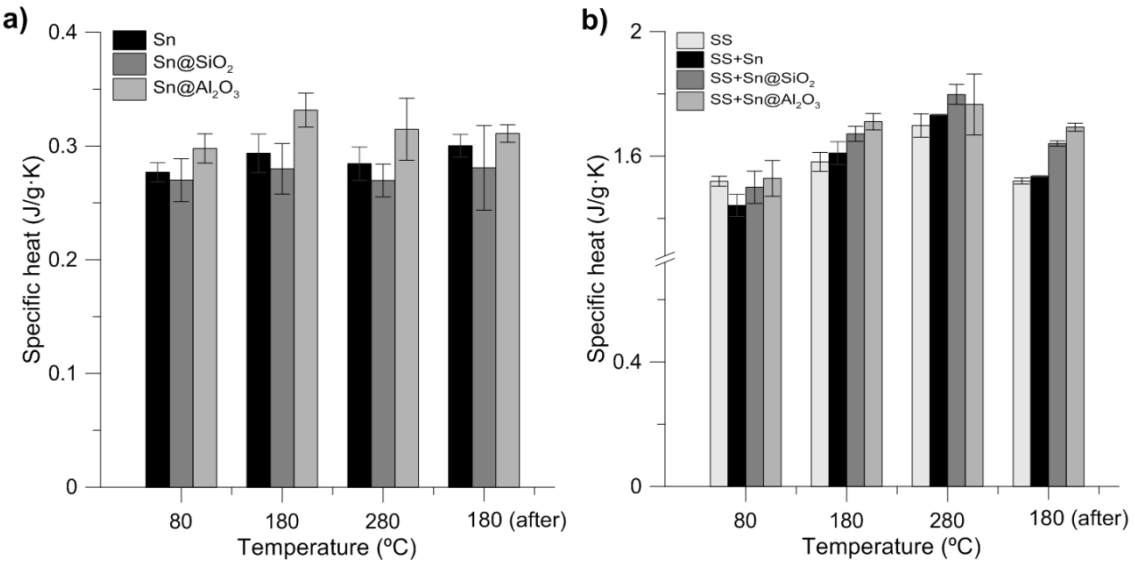

Figure 13. Specific heat of a) nePCMs and b) Solar salt based nanofluids at 1 wt.%

Table 4. Specific heat variation for the nePCMs and the nanofluids at 1 wt.%

T (ºC)	80	180	280	180 (after)
Sample	**Variation**	**Variation**	**Variation**	**Variation**
Sn	-	-	-	-
Sn@SiO_2	-2.52%	-4.67%	-5.18%	-6.52%
Sn@Al_2O_3	+7.56%	+12.92%	+10.65%	+10.79%
SS	-	-	-	-
SS+ Sn	-5.09%	+1.79%	+2.02%	+0.99%
SS+ Sn@SiO_2	-1.26%	+5.69%	+5.88%	+7.93%
SS+ Sn@Al_2O_3	+0.62%	+8.16%	+3.99%	+11.38%

Thermal energy storage capacity is defined as the addition of sensible heat storage and latent heat storage. For any TES material it can be calculated as:

$$Q_{total} = Q_{sensible} + Q_{latent} = m \cdot c_P \cdot \Delta T + m \cdot \Delta H \quad (1)$$

where m refers to the mass of the material, c_p to its specific heat, ΔT to the temperature step studied, and ΔH to its phase change enthalpy.

The enhancement of the thermal energy storage of the nanofluids with respect to the base fluid alone have been calculated using the values of specific heat and fusion enthalpy of the nanofluids and the base fluid alone, previously measured, according to Equation 2.

$$\Delta Q_{total} = \frac{m_{nf}(c_{P,nf} \cdot \Delta T + \Delta H_{nf})}{m_{bf}(c_{P,bf} \cdot \Delta T + \Delta H_{bf})} = \frac{\rho_{nf} \cdot V_{nf}(c_{P,nf} \cdot \Delta T + \Delta H_{nf})}{\rho_{bf} \cdot V_{bf}(c_{P,bf} \cdot \Delta T + \Delta H_{bf})} \quad (2)$$

where the subscript *bf* refers to the base fluid properties, ρ is the density and V is the volume.

The thermal energy storage enhancement was compared assuming constant mass ($m_{nf} = m_{bf}$) and constant volume ($V_{nf} = V_{bf}$) of the TES material (nanofluid and base fluid, respectively) at the same working temperature (including the phase change) and with a mass loading of nePCMs of 1 wt.%. The results are presented in Table 5, where it is

observed that the addition of nePCMs improves the thermal energy storage capacity for all the cases studied, due to a combination of the enhancement in the specific heat when adding nePCM and to the contribution of latent heat. Temperature steps of 150 ºC, 180 ºC and 200 ºC have been studied according to working cycles possible in a real application. It can also be noticed that the higher increments are for the nanofluids containing the ALD coated nePCMs, that present a higher specific heat value and thus a higher sensible heat contribution than the combination of solar salt with Sn nePCMs. It is also remarkable that the enhancement is always higher for the ALD coated Sn@Al_2O_3 nePCMs, which in addition to the previously observed enhanced thermal stability will result in a promising alternative to the commonly used TES materials.

Table 5. Thermal energy storage enhancement of the nanofluids compared to the base fluid (SS).

	Constant mass			**Constant volume**		
Nanofluid	**ΔT = 150ºC**	**ΔT = 180ºC**	**ΔT = 200ºC**	**ΔT = 150ºC**	**ΔT = 180ºC**	**ΔT = 200ºC**
SS+ Sn	+0.28%	+0.36%	+0.41%	+1.05%	+1.13%	+1.18%
SS+ Sn@SiO_2	+6.63%	+6.77%	+6.86%	+7.33%	+7.48%	+7.56%
SS+ Sn@Al_2O_3	+9.42%	+9.64%	+9.77%	+10.12%	+10.35%	+10.47%

5. Conclusions

Multi-coated nePCMs consisting of Sn/SnO_x nanoparticles coated with SiO_2 and Al_2O_3 have been synthesised by Atomic Layer Deposition. The suitability of ALD to deposit uniform and conformal coatings with thicknesses of approximately 8 nm of SiO_2 and 10 nm of Al_2O_3 on the nanoparticles after 50 coating cycles was proved. The oxidation state of the native tin oxide on the nePCMs changed due to the ALD coating on the Sn@SiO_2 samples from SnO to SnO_2 when subject to high temperatures, while it remained as SnO in the Sn@Al_2O_3. Both SiO_2 and Al_2O_3 coatings were amorphous and retained their structure up to 280 ºC. The resistance to the oxidation of the Sn core of

the nePCM improved with the ALD coatings when the samples were subject to thermal cycling in nitrogen. This enhancement is especially high for $Sn@Al_2O_3$ samples, which also showed an enhanced resistance to oxidation under thermal cycling in an oxidising atmosphere. This results in an enhanced stability of the latent heat storage capacity of the nePCMs, which can be of use in nanofluids for thermal energy storage. The sensible heat storage capacity of the ALD coated nePCMs was tested by preparing nanofluids based on solar salt. The nanofluids prepared with the nePCM coated with 50 cycles of SiO_2 and Al_2O_3 showed an increase on their specific heat up to 11.4%. This, combined with the previously stated contribution of the nePCMs to latent heat, will translate into an overall enhanced thermal energy storage capacity of the nanofluids when the nePCM were coated, especially in the case of Al_2O_3 coated nanoparticles which allow for enhancements of up to 10.5% with respect to the solar salt.

Acknowledgements

The authors want to thank the financial support from Ministerio de Economía y Competitividad (MINECO) (project ENE2016-77694-R) and Universitat Jaume I (project UJI-B2016-47). Nuria Navarrete thanks Universitat Jaume I for a pre-doctoral fellowship (Ref. PREDOC/2016/28) and a research mobility grant (Ref. E-2018-10) that made possible the research carried out in this work. Authors thank Servicios Centrales de Instrumentacion Científica (SCIC) of Universitat Jaume I for the use of TEM (Maria del Carmen Peiro), FT-IR (José Miguel Pedra), XRD (Gabriel Peris), TGA and DSC (Cristina Zahonero). This work has been developed by participants of the COST Action CA15119 Overcoming Barriers to Nanofluids Market Uptake (NANOUPTAKE).

References

[1] G. Alva, Y. Lin, and G. Fang, "An overview of thermal energy storage systems," *Energy*, vol. 144. Pergamon, pp. 341–378, 01-Feb-2018.

[2] X. Luo, J. Wang, M. Dooner, and J. Clarke, "Overview of current development in electrical energy storage technologies and the application potential in power system operation," *Appl. Energy*, vol. 137, pp. 511–536, Jan. 2015.

[3] E. Oró, A. Gil, A. de Gracia, D. Boer, and L. F. Cabeza, "Comparative life cycle assessment of thermal energy storage systems for solar power plants," *Renew. Energy*, vol. 44, pp. 166–173, Aug. 2012.

[4] N. Pfleger, T. Bauer, C. Martin, M. Eck, and A. Wörner, "Thermal energy storage - overview and specific insight into nitrate salts for sensible and latent heat storage," *Beilstein J. Nanotechnol.*, vol. 6, no. 1, pp. 1487–1497, 2015.

[5] G. Wei *et al.*, "Selection principles and thermophysical properties of high temperature phase change materials for thermal energy storage: A review," *Renew. Sustain. Energy Rev.*, vol. 81, no. March 2017, pp. 1771–1786, Jan. 2018.

[6] S. Khare, M. Dell'Amico, C. Knight, and S. McGarry, "Selection of materials for high temperature latent heat energy storage," *Sol. Energy Mater. Sol. Cells*, vol. 107, pp. 20–27, Dec. 2012.

[7] B. Zalba, J. M. Marín, L. F. Cabeza, and H. Mehling, "Review on thermal energy storage with phase change: Materials, heat transfer analysis and applications," *Applied Thermal Engineering*, vol. 23, no. 3. Pergamon, pp. 251–283, 01-Feb-2003.

[8] A. Sharma, V. V. Tyagi, C. R. Chen, and D. Buddhi, "Review on thermal energy storage with phase change materials and applications," *Renewable and Sustainable Energy Reviews*, vol. 13, no. 2. Pergamon, pp. 318–345, 01-Feb-

2009.

[9] H. Liu, X. Wang, and D. Wu, “Innovative design of microencapsulated phase change materials for thermal energy storage and versatile applications: A review,” *Sustain. Energy Fuels*, vol. 3, no. 5, pp. 1091–1149, 2019.

[10] R. Taylor *et al.*, “Small particles, big impacts: A review of the diverse applications of nanofluids,” *J. Appl. Phys.*, vol. 113, no. 1, 2013.

[11] M. Chieruzzi, G. F. Cerritelli, A. Miliozzi, and J. M. Kenny, “Effect of nanoparticles on heat capacity of nanofluids based on molten salts as PCM for thermal energy storage,” *Nanoscale Res. Lett.*, vol. 8, no. 1, pp. 1–9, 2013.

[12] H. Riazi, T. Murphy, G. B. Webber, R. Atkin, S. S. M. Tehrani, and R. A. Taylor, “Specific heat control of nanofluids: A critical review,” *Int. J. Therm. Sci.*, vol. 107, pp. 25–38, 2016.

[13] P. Andreu-Cabedo, R. Mondragon, L. Hernandez, R. Martinez-Cuenca, L. Cabedo, and J. E. Julia, “Increment of specific heat of Solar Salt with SiO2 and Al2O3 nanoparticles,” *Nanoscale Res. Lett.*, vol. 9, no. 1, p. 582, 2014.

[14] R. Mondragón, J. E. Juliá, L. Cabedo, and N. Navarrete, “On the relationship between the specific heat enhancement of salt-based nanofluids and the ionic exchange capacity of nanoparticles,” *Sci. Rep.*, vol. 8, no. 1, pp. 1–12, 2018.

[15] M. M. Zhang *et al.*, “Encapsulated nano-heat-sinks for thermal management of heterogeneous chemical reactions.,” *Nanoscale*, vol. 2, no. 12, pp. 2790–2797, 2010.

[16] A. Hassan, M. S. Laghari, and Y. Rashid, “Micro-encapsulated phase change materials: A review of encapsulation, safety and thermal characteristics,” *Sustain.*, vol. 8, no. 10, 2016.

[17] Y. E. Milián, A. Gutiérrez, M. Grágeda, and S. Ushak, “A review on

encapsulation techniques for inorganic phase change materials and the influence on their thermophysical properties," *Renew. Sustain. Energy Rev.*, vol. 73, no. December 2016, pp. 983–999, 2017.

[18] N. Navarrete *et al.*, "Nanofluid based on self-nanoencapsulated metal/metal alloys phase change materials with tuneable crystallisation temperature," *Sci. Rep.*, vol. 7, no. 1, pp. 1–10, 2017.

[19] N. Navarrete, R. Mondragón, D. Wen, M. E. Navarro, Y. Ding, and J. E. Juliá, "Thermal energy storage of molten salt –based nanofluid containing nano-encapsulated metal alloy phase change materials," *Energy*, vol. 167, pp. 912–920, 2019.

[20] H. Van Bui, F. Grillo, and J. R. Van Ommen, "Atomic and molecular layer deposition: off the beaten track," *Chem. Commun.*, vol. 53, no. 1, pp. 45–71, 2017.

[21] J. R. Wank, S. M. George, and A. W. Weimer, "Coating fine nickel particles with Al2O3 utilizing an atomic layer deposition-fluidized bed reactor (ALD-FBR)," *J. Am. Ceram. Soc.*, vol. 87, no. 4, pp. 762–765, 2004.

[22] M. A. Weimer *et al.*, "Ultrafast metal-insulator varistors based on tunable Al2 O3 tunnel junctions," *Appl. Phys. Lett.*, vol. 92, no. 16, pp. 1–4, 2008.

[23] D. M. King, Y. Zhou, L. F. Hakim, X. Liang, P. Li, and A. W. Weimer, "In situ synthesis of TiO 2-functionalized metal nanoparticles," *Ind. Eng. Chem. Res.*, vol. 48, no. 1, pp. 352–360, 2009.

[24] O. J. Kilbury *et al.*, "Atomic layer deposition of solid lubricating coatings on particles," *Powder Technol.*, vol. 221, pp. 26–35, 2012.

[25] P. Uudeküll *et al.*, "Atomic layer deposition of titanium oxide films on As-synthesized magnetic Ni particles: Magnetic and safety properties," *J. Magn.*

Magn. Mater., vol. 429, pp. 299–304, May 2017.

[26] S. Zhang *et al.*, "Helium interactions with alumina formed by atomic layer deposition show potential for mitigating problems with excess helium in spent nuclear fuel," *J. Nucl. Mater.*, vol. 499, pp. 301–311, 2018.

[27] B. Moghtaderi, I. Shames, and E. Doroodchi, "Combustion prevention of iron powders by a novel coating method," *Chem. Eng. Technol.*, vol. 29, no. 1, pp. 97–103, 2006.

[28] L. F. Hakim *et al.*, "Synthesis of oxidation-resistant metal nanoparticles via atomic layer deposition," *Nanotechnology*, vol. 18, no. 34, p. 345603, Aug. 2007.

[29] Y. Zhou, D. M. King, J. Li, K. S. Barrett, R. B. Goldfarb, and A. W. Weimer, "Synthesis of photoactive magnetic nanoparticles with atomic layer deposition," *Ind. Eng. Chem. Res.*, vol. 49, no. 15, pp. 6964–6971, 2010.

[30] V. Cremers *et al.*, "Oxidation barrier of Cu and Fe powder by atomic layer deposition," *Surf. Coatings Technol.*, no. 349, pp. 1032–1041, 2018.

[31] J. D. Ferguson, K. J. Buechler, A. W. Weimer, and S. M. George, "SnO2 atomic layer deposition on ZrO2 and Al nanoparticles: Pathway to enhanced thermite materials," in *Powder Technology*, 2005, vol. 156, no. 2–3, pp. 154–163.

[32] L. Qin, T. Gong, H. Hao, K. Wang, and H. Feng, "Core-shell-structured nanothermites synthesized by atomic layer deposition," *J. Nanoparticle Res.*, vol. 15, no. 12, 2013.

[33] L. Qin, N. Yan, J. Li, H. Hao, F. Zhao, and H. Feng, "Enhanced energy performance from core-shell structured Al@Fe2O3 nanothermite fabricated by atomic layer deposition," *RSC Adv.*, vol. 7, no. 12, pp. 7188–7197, 2017.

[34] K. Manandhar, J. A. Wollmershauser, J. E. Boercker, and B. N. Feigelson, "Growth per cycle of alumina atomic layer deposition on nano- and micro-

powders," *J. Vac. Sci. Technol. A Vacuum, Surfaces, Film.*, vol. 34, no. 2, p. 021519, 2016.

[35] R. Beetstra, U. Lafont, J. Nijenhuis, E. M. Kelder, and J. R. Van Ommen, "Atmospheric pressure process for coating particles using atomic layer deposition," *Chem. Vap. Depos.*, vol. 15, no. 7–9, pp. 227–233, 2009.

[36] G. Ferrer, C. Barreneche, A. Solé, I. Martorell, and L. F. Cabeza, "New proposed methodology for specific heat capacity determination of materials for thermal energy storage (TES) by DSC," *J. Energy Storage*, vol. 11, pp. 1–6, 2017.

[37] J. D. Ferguson, A. W. Weimer, and S. M. George, "Atomic layer deposition of SiO2 films on BN particles using sequential surface reactions," *Chem. Mater.*, vol. 12, no. 11, pp. 3472–3480, 2000.

[38] G. Socrates, *Infrared and Raman Characteristic Group Frequencies: Tables and Charts*, 3rd editio. John Wiley & Sons, LTD, 2004.

[39] D. N. Goldstein, J. A. McCormick, and S. M. George, "Al2O3Atomic layer deposition with trimethylaluminum and ozone studied by in situ transmission FTIR spectroscopy and quadrupole mass spectrometry," *J. Phys. Chem. C*, vol. 112, no. 49, pp. 19530–19539, 2008.

[40] D. Valdesueiro, G. M. H. Meesters, M. T. Kreutzer, and J. R. van Ommen, "Gas-phase deposition of ultrathin aluminium oxide films on nanoparticles at ambient conditions," *Materials.*, vol. 8, no. 3, pp. 1249–1263, 2015.

[41] D. Zhang, D. La Zara, M. J. Quayle, G. Petersson, and J. R. Van Ommen, "Nanoengineering of Crystal and Amorphous Surfaces of Pharmaceutical Particles for Biomedical Applications," 2019.

[42] Y. Hong *et al.*, "Controlling super-cooling of encapsulated phase change nanoparticles for enhanced heat transfer," *Chem. Phys. Lett.*, vol. 504, no. 4–6,

pp. 180–184, 2011.